Gene Expression, Vol. 19, pp. 97–119
Printed in the USA.

1052-2166/19 $90.00 + .00
DOI: https://doi.org/10.3727/105221618X15361728786767
E-ISSN 1555-3884
www.cognizantcommunication.com

Single-Cell Gene Expression Analysis Identifies Chronic Alcohol-Mediated Shift in Hepatocyte Molecular States After Partial Hepatectomy

Sirisha Achanta,* Aalap Verma,*† Ankita Srivastava,* Harshavardhan Nilakantan,* Jan B. Hoek,* and Rajanikanth Vadigepalli*

*Daniel Baugh Institute for Functional Genomics and Computational Biology, Department of Pathology, Anatomy and Cell Biology, Thomas Jefferson University, Philadelphia, PA, USA
†Department of Biomedical Engineering, University of Delaware, Newark, DE, USA

The analysis of molecular states of individual cells, as defined by their mRNA expression profiles and protein composition, has gained widespread interest in studying biological phenomena ranging from embryonic development to homeostatic tissue function and genesis and evolution of cancers. Although the molecular content of individual cells in a tissue can vary widely, their molecular states tend to be constrained within a transcriptional landscape partly described by the canonical archetypes of a population of cells. In this study, we sought to characterize the effects of an acute (partial hepatectomy) and chronic (alcohol consumption) perturbation on the molecular states of individual hepatocytes during the onset and progression of liver regeneration. We analyzed the expression of 84 genes across 233 individual hepatocytes acquired using laser capture microdissection. Analysis of the single-cell data revealed that hepatocyte molecular states can be considered as distributed across a set of four states irrespective of perturbation, with the proportions of hepatocytes in these states being dependent on the perturbation. In addition to the quiescent, primed, and replicating hepatocytes, we identified a fourth molecular state lying between the primed and replicating subpopulations. Comparison of the proportions of hepatocytes from each experimental condition in these four molecular states suggested that, in addition to aberrant priming, a slower transition from primed to replication state could contribute toward ethanol-mediated suppression of liver regenerative response to partial hepatectomy.

Key words: Liver regeneration; Partial hepatectomy; Hepatocyte biology; Cell and molecular biology; Alcohol-induced liver injury—chronic; Nonalcoholic fatty liver disease (NAFLD)

INTRODUCTION

Recent developments in high-throughput single-cell technologies have enabled the measurement of gene expression and proteomic profiles at an unprecedented resolution. Single-cell-level studies on a wide array of cell types from diverse organ systems, disease contexts, and perturbations have revealed a high degree of variability in mRNA and protein expression of individual cells[1–3]. Despite this large variability, it has been argued that mRNA expression and protein profiles of individual cells, termed as their molecular state, are not randomly distributed but are likely tuned along a gradient between gene expression patterns observed in canonical archetypes[4–6]. An emerging view is that molecular states of cells are dynamic and arise due to their interactions with their microenvironments within developing as well as differentiated tissue. Several factors can contribute toward shaping the extracellular microenvironment, such as inputs[5], spatial location[7], developmental stage[8], injury[9], and other intrinsic and extrinsic factors. Owing to extensive interactions between cells and their microenvironments, analyzing the molecular states of a population of cells could reveal valuable information about the functional state and history of not just the specific cells under investigation but the tissue as a whole. For instance, a recent single hepatocyte RNA-seq study in mouse liver[10] identified zonal heterogeneity patterns and possible regulators of in vivo spatial mRNA expression heterogeneity in mouse liver lobules.

The underlying molecular heterogeneity structure of single-cell populations in a tissue can change due to acute or chronic perturbations. Molecular state heterogeneity of individual cells under homeostatic conditions could be a crucial determinant of tissue fate after perturbations.

Address correspondence to Rajanikanth Vadigepalli, Daniel Baugh Institute for Functional Genomics and Computational Biology, Department of Pathology, Anatomy and Cell Biology, Thomas Jefferson University, 1020 Locust Street, Room 314, Philadelphia, PA 19107, USA. Tel: 215-955-0576; Fax: 215-503-2636; E-mail: rajanikanth.vadigepalli@jefferson.edu

For example, inherently heterogeneous neural stem cell populations residing in adult subventricular zone get activated due to ischemia, potentially contributing to the diversity of neural and glial fates[9]. Here we consider a chronic perturbation (adaptation to ethanol intake) and an acute challenge (partial hepatectomy) to examine the effects on the distribution of single-cell gene expression in the liver. Adaptation to chronic ethanol intake is known to activate various stress response programs and lead to dysregulation of liver repair mechanisms[11,12]. Previous studies have shown that liver gene expression shows an adaptive response to chronic ethanol feeding with only moderate changes in steady state gene expression in rats[13]. However, these observations are based on data collected from whole tissue samples and hence cannot provide insights on the changes in the single-cell gene expression in the liver tissue. We address this gap in the present study by developing and analyzing high-throughput data on hepatoctye gene expression profiles at the single-cell scale.

In addition to adaptation to a chronic perturbation (alcohol intake), we also considered an acute challenge of partial hepatectomy, to evaluate the changes in gene expression heterogeneity and the corresponding hepatocyte molecular states. After partial hepatectomy (PHx), a complex interplay between the different liver cell types and extracellular matrix leads to a coordinated regenerative response[14–17]. Liver regeneration response to PHx is suppressed during the initial stages in a rat model of adaptation to chronic ethanol intake[18]. We evaluated the changes in the single-cell gene expression profiles induced by adaptation to ethanol intake, as well as the impact of PHx on the distribution of hepatocyte molecular states. We utilized a combination of clustering and template-matching approach to partition the single hepatocytes into distinct molecular states based on gene expression profiles. Our analysis identified distinct hepatocyte molecular states that were present in the ethanol-adapted and acute PHx response groups, at different proportions across the experimental conditions. Our results showed expected differences in the proportion of proliferative cell states after PHx between ethanol and control groups. In addition, our analysis revealed that adaptation to ethanol intake promotes the primed and transitional hepatocyte molecular states at the expense of the quiescent and proliferative states. These results suggest a stimulated-but-stalled scenario as underlying the ethanol-mediated deficit in the liver regenerative response to partial hepatectomy.

MATERIALS AND METHODS

Single Hepatocyte Sample Acquisition

In this study, we used four male, adult (8–10 weeks old) Sprague–Dawley rats (*Rattus norvegicus*) (see Fig. 1 for the experimental design). The rats were subjected to the Lieber–DeCarli pair feeding protocol to induce adaptation to chronic ethanol intake[19], with two animals receiving alcohol-containing liquid diet and two animals receiving carbohydrate control liquid diet. The alcohol diet contained 36% of total calories derived from ethanol (6.2% v/v). Littermate control rats were pair fed with liquid diet in which ethanol was replaced isocalorically by carbohydrate (maltose–dextran). The animals were held in single occupancy cages in a climate-controlled, 12-h day/night cycle in accordance with acceptable animal handling practices.

Following 5 weeks of pair feeding, rats were anesthetized and subjected to 70% PHx following the protocol described in Crumm et al.[20]. The left lateral and medial lobes (LLM) were removed and quickly frozen in OCT blocks (Sakura Finetek USA, Torrance, CA, USA) over dry ice. Twenty-four hours after PHx, the rats were anesthetized again. The original incision was reopened, and the remnant liver was harvested as before. Following this surgery, the animals were sacrificed by exsanguination. The harvested tissue was frozen on dry ice and stored at −80°C. All surgeries were performed between 8 AM and 11 AM in order to minimize circadian rhythm effects. All animal handling and surgical procedures were approved by the Institutional Animal Care and Use Committee (IACUC) at Thomas Jefferson University.

Tissue Staining

Frozen liver tissue in OCT blocks was sectioned into 10-μm-thick slices using a clean, RNase inhibitor-treated cryostat at −20°C. Sliced tissue was stored up to a maximum of 2 weeks. Tissue staining was performed using a rapid staining protocol, taking approximately 30 min, to preserve RNA integrity. In this approach, slides were first fixed in cold acetone and hydrogen peroxide (50 ml: 50 μl; Sigma-Aldrich, St. Louis, MO, USA) for 30 s. The slides were washed and then incubated for 4 min at room temperature in the dark with DAPI 1:10,000, phalloidin 2.5:100, and PBS containing 2% BSA. The slides were then rinsed with PBS and dehydrated in graduated ethanol concentrations (70–100%) and in xylene for 5 min.

Laser Capture Microdissection

The laser capture microdissection (LCM) process was performed using the PixCell system and CapSure Macro LCM caps (Arcturus Engineering, Mountain View, CA, USA). Single hepatocytes showing positive nuclear stain (DAPI) surrounded by cell membrane (phalloidin) 7–10 cell layers away from the central vein and the portal triad were identified by their size and morphology and lifted individually on caps. The annulus for the laser was adjusted to the size of hepatocytes (approximately 20 μm). During single-cell sample collection the tissue section

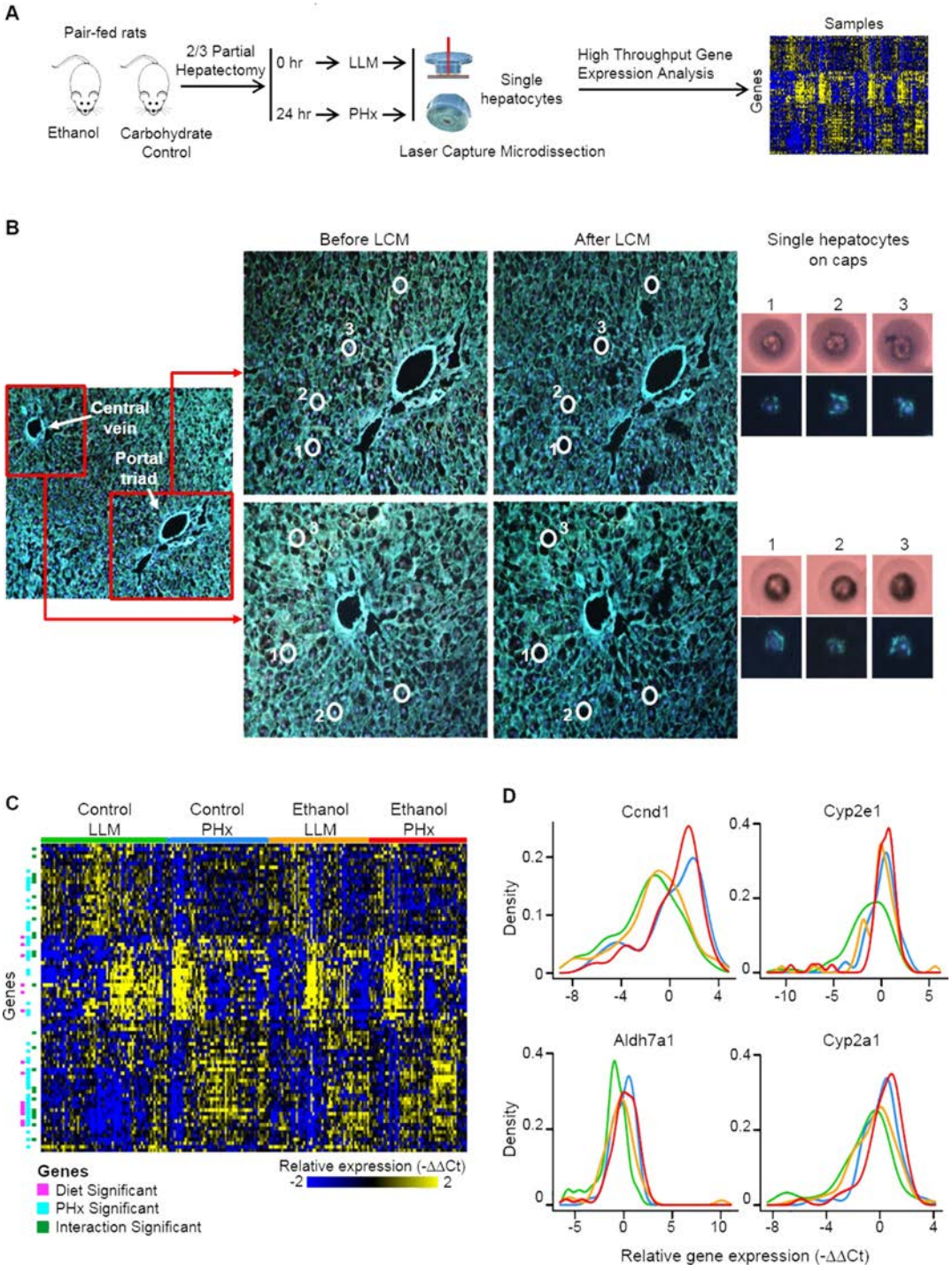

Figure 1. Gene expression in single hepatocytes. (A) Workflow schematic of our experimental approach to obtain single hepatocyte gene expression data. (B) Single hepatocyte lifting using laser capture microdissection (LCM) from 10-µm-thick liver sections stained with DAPI and phalloidin. Sections of the tissue are shown before and after cell lifting. Fluorescence from the single lifted hepatocytes can be visualized on caps. (C) Despite large variability, gene expression across groups of single hepatocytes exhibits significant differences as seen in the heat map of gene expression data in this study highlighting two-way ANOVA results. Diet-significant, time-significant (0 h and 24 h postregeneration), and interaction-significant genes across all the four conditions highlighted. Consistent with expectation, a large number of genes show significant differences after partial hepatectomy (PHx). (D) Shifts in distributions of gene expression in groups of single hepatocytes are consistent with expectation. Ccnd1 expression increases after PHx in control as well as ethanol samples. Alcohol and aldehyde metabolism genes Cy2e1, Aldh7a1, and Cyp2a1 show lower expression in control LLM samples.

as well as the corresponding cap were inspected for the removed cell body to ensure that the fluorescent hepatocyte of interest was collected. Lysis buffer was added onto the single cell on the cap (5.5 µl; Life Technologies, Grand Island, NY, USA) and cooled on ice before storage at −80°C.

High-Throughput qPCR

Single hepatocytes in lysis buffer were directly processed for reverse transcriptase reaction using SuperScript VILO Master Mix (Thermo Fisher Scientific, Waltham, MA), followed by real-time PCR for targeted amplification and detection using the Evagreen intercalated dye-based approach to detect the PCR-amplified product.

Intron-spanning PCR primers were designed for every assay using Primer3[21,22] and BLAST[23]. Genes were selected from across a wide array of liver functions relevant to chronic ethanol exposure and PHx. The raw and normalized dataset has been made available online as a Gene Expression Omnibus dataset (GEO reference ID: GSE111448). The standard BioMark protocol was used to preamplify cDNA samples for 22 cycles using TaqMan PreAmp Master Mix as per the manufacturer's protocol[5] (Applied Biosystems, Foster City, CA, USA). qPCR reactions were performed using 96.96 BioMark Dynamic Arrays (Fluidigm, South San Francisco, CA, USA) enabling quantitative measurement of multiple mRNAs and samples under identical reaction conditions. Each run consisted of 30 amplification cycles (15 s at 95°C, 5 s at 70°C, 60 s at 60°C). Ct values were calculated by the Real-Time PCR Analysis Software (Fluidigm). Four 96 × 96 BioMark Arrays were used to measure gene expression across the 318 single-cell samples. The same serial dilution sample set was included in each chip to verify reproducibility and test for technical variability on each Biomark array. A chip-to-chip comparison of the serial dilution samples demonstrates that the BioMark Dynamic Arrays are capable of high reproducibility with minimal technical variability (Fig. 2).

Immunofluorescence Staining

Frozen liver tissues sectioned at 20-µm thickness were used for immunofluorescence. Liver tissue stored at −80°C was sliced into 20-µm-thick sections. The tissue

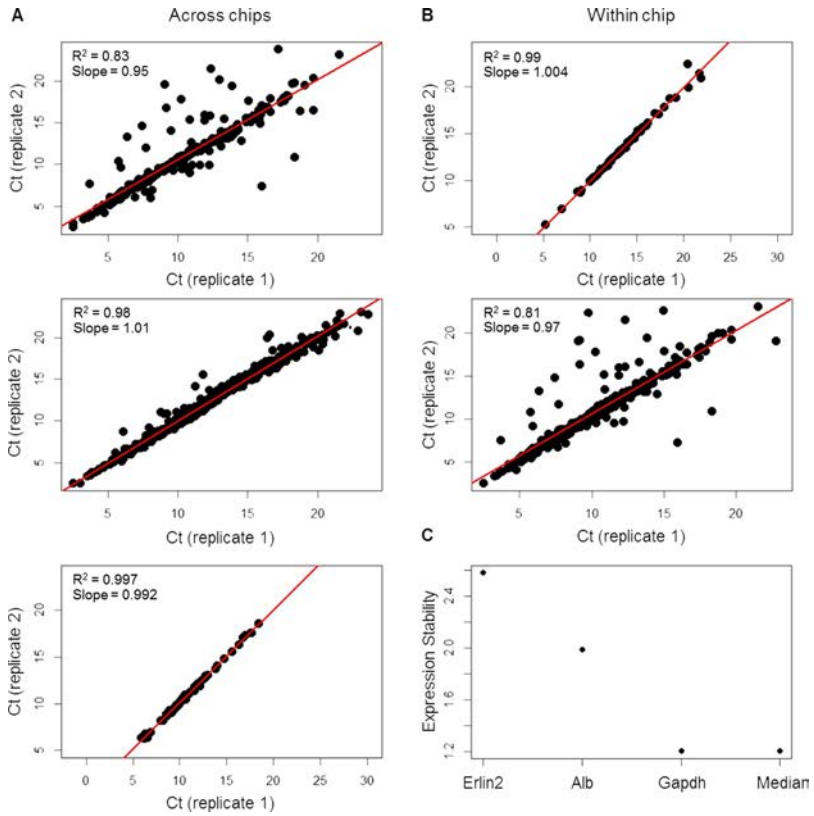

Figure 2. Technical reproducibility and normalization in single-cell qPCR experiments. Ct values for repeated reactions across different BioMark chips (A) as well as within a chip (B) suggest a high degree of reproducibility. (C) Comparison of gene stability for three candidate reference genes and the median sample expression obtained using 55 high-performing genes. Reference gene selection procedure described in Vandesompele et al.[26] suggested that the median sample expression across 55 high-performing genes is the most suited for within-sample normalization.

sections were fixed in 4% paraformaldehyde (Electron Microscopy Sciences, Hatfield, PA, USA) and washed with 1× PBS (Fisher Bioreagents), three washes for 5 min each. The tissue sections were permeabilized using Triton X-100 (LabChem, Zelienople, PA, USA) at a concentration of 0.02% for 15 min, followed by two washes of 5 min each with 1× PBS. The permeabilized sections were then blocked using 5% normal goat serum (ab7481; Abcam, Cambridge, MA, USA) for 1 h. All steps including fixation and blocking were done at room temperature. Slides with liver tissue sections were incubated overnight at 4°C followed by three washes of 1× PBS at 5-min interval each. The primary antibody comprised pStat3 (9145; 1:100; Cell Signaling, Danvers, MA, USA) and anti-Socs3 antibody (ab16030; 1:100; Abcam). The secondary antibodies used for staining purposes at 1:500 dilutions included goat anti-rabbit IgG Alexa Fluor 555 (ab150086; Abcam). The tissue sections on slides were incubated with secondary antibody for 1 h 45 min at room temperature followed by three washes of 5 min each with 1× PBS. After secondary antibody incubation, DAPI (D9542; Sigma-Aldrich) and Alexa Fluor-488-conjugated phalloidin (A12379; Life Technologies, Carlsbad, CA, USA) were applied together and allowed to incubate for 15 min followed by three washes of 5 min each. ProLong Diamond Antifade (Life Technologies) solution was applied, and the slides were mounted with coverslips. Prior to microscopic imaging, slides were cured at room temperature overnight. Negative controls in the absence of the primary antibody showed negligible signal intensity.

Confocal Imaging

Images were acquired using a Zeiss LSM 780 mounted on a Zeiss Axio Observer inverted microscope. Zeiss ZEN 2011 software package associated with the LSM 780 was used to capture images. The lasers 405 nm, 488 nm, and 555 nm were used for image acquisition, having been set with a unique and high-contrast color for each channel. The detectors in Zeiss ZEN 2011 were set at a specific standard available for a specific dye. Two tracks were created with the best signal in a manner that there would be no interference between laser channels.

The 405-nm laser was used to capture DAPI, the 488-nm was used to illuminate the Alexa Fluor 488 phalloidin, and the 555-nm was aimed at exciting the A555 conjugated anti-rabbit/mouse secondary. Images were acquired at a pixel resolution of 1024 × 1024, at 8-bit color depth with a line scan and averaging intensities from four scans of the same area. Prior to acquisitions, saturation and zeros were set using the range indicator.

Digital Image Analysis

The image analysis was performed using a custom analysis pipeline developed in CellProfiler[24]. All channels in each multiplexed immunostained image were converted into an 8-bit grayscale image. Automated thresholding was performed on the DAPI grayscale image to segment hepatocyte nuclei and subsequently develop a mask corresponding to hepatocyte nuclei. The nuclear mask was then applied to the pSTAT3 (or SOCS3) grayscale image to measure nuclear protein intensities. Similarly, cytosolic/cell masks for hepatocytes were developed using a combination of the DAPI and phalloidin grayscale images, and subsequently applied to pSTAT3 (or SOCS3) channel grayscale images to measure cytosolic/whole cell intensities.

Western Blotting

The baseline and 24-h PHx liver tissue samples were freeze clamped and stored at −80°C prior to use. The tissue homogenization was carried out in cold conditions using RIPA lysis buffer (89900; Life Technologies) supplemented with Halt Phosphatase Inhibitor Cocktail (7842; Life Technologies) and Halt™ Protease Inhibitor Cocktail (87785; Life Technologies). Protein estimation from tissue lysate was performed using Pierce BCA Protein Assay Kit (23227; Life Technologies), and an equal amount of protein run on 8% or 12% SDS-PAGE (Mini-Protean; Bio-Rad, Richmond, CA, USA). Resolved proteins were blotted to Immun-Blot PVDF membrane (Bio-Rad), blocked with 5% Blotting-Grade Blocker (1706404; Bio-Rad), and incubated with primary Ab at 4°C overnight.

The antibodies used for primary overnight incubation were pStat3 (9145; 1:500; Cell Signaling, Danvers, MA, USA), STAT3 (9139; ;1:1,000; Cell Signaling), anti-Socs3 antibody (ab16030; ; 1:1,000; Abcam), and GAPDH (MAB374; 1:1,000; Millipore). The membrane was washed with TBST [25 mM Tris (pH 7.60), 137 mM NaCl, and 0.1% Tween 20] and probed with HRP-conjugated secondary Ab. Immunoreactive bands were visualized on Kodak Image Station 440CF by chemiluminescent Clarity™ Western ECL Substrate (1705060; Bio-Rad).

Single-Cell qRT-PCR Data Normalization

Individual qRT-PCR results were examined to determine the quality of the qRT-PCR. An initial pass-fail-no call assessment was made for each reaction based on the qualitative nature of the reaction curves obtained from the PCR. Following this initial review, both samples and gene assays with >40% failed reactions (84 single cell samples and 12 genes) were excluded from the present analysis. Upon filtering based on these criteria, a total of 233 single-cell samples (69 baseline control samples, 55 control PHx samples, 55 baseline ethanol samples, and 54 ethanol PHx samples) and 84 different gene assays were carried forward in the present analysis. Raw Ct values for individual samples were normalized against a

median expression level of subset of 55 high-expressing genes to obtain − Ct values. All genes with high-quality data in >60% of the samples in each condition were included in the pool of high-expressing genes to obtain − Ct values. The following equation was used to calculate − Ct values for each gene: $-Ct_{gene}$ = (median sample expression) $- Ct_{gene}$.

The vector of median sample expression value was chosen over potential reference genes based on previously developed microarray data normalization methods[25,26]. Based on our analysis, the median sample expression exhibited the highest stability measure and was therefore picked for normalization.

The − Ct data were then rescaled using the median across all samples within a gene for all chips using the following equation: $-Ct_{gene} = -Ct_{sample}$ (across-sample − Ct median).

Imputation of Gene Expression Data

Our data consisted of 26.5% missing values after quality control and normalization. We imputed the missing values in the normalized dataset using a k-nearest neighbor imputation approach[27].

Template Matching qRT-PCR Data

Hepatocytes were separated into different subpopulations based on their molecular profiles using an implementation of the template matching method[28] in Multi Experiment Viewer[29]. Briefly, template matching estimates the correlation between a rescaled expression profile used as the template and a test expression profile. Control baseline samples were hierarchically clustered to obtain the canonical subpopulations. The canonical subpopulations were identified in control baseline samples using hierarchical clustering (Pearson correlation, complete linkage) with a dissimilarity threshold of 1.089, yielding seven sample clusters. The average silhouette width for all clusters (estimated using the cluster package in R) was 0.11, significantly higher than 1,000 randomized trials (Fig. 3). These sample clusters were divided into four different subpopulations. Gene medians of these subpopulations were used as templates to classify the hepatocytes from other conditions (control PHx, ethanol LLM, and ethanol PHx) into one of the canonical subpopulations. We used a *p* value-based cutoff for our template match analysis (threshold *p* value = 0.05). Hepatocytes that did not pass the *p* value threshold for any of the canonical templates were divided into new clusters using hierarchical clustering. Functional identification of the subpopulations was performed based on expression levels of key gene markers (see Results).

Statistical Comparison of Cell State Proportions

Proportions of samples from each condition lying in the molecular states identified in the single-cell qRT-PCR data were compared using Pearson's chi-squared test in R (packages *stats* and *NCStats*).

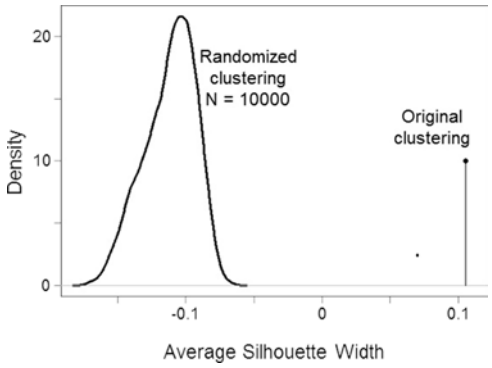

Figure 3. Comparison of silhouette widths of the original clusters in our data with 10,000 randomized clusters of the same sizes ($p < 2.2e{-}16$). The original clusters were obtained using Pearson correlation-based hierarchical clustering (complete linkage) on control LLM samples yielding a silhouette score of 0.11. The samples were then randomly assigned to different clusters of the same sizes as those obtained in the original clustering, and silhouette coefficients were estimated for the randomized clusters ($N = 10{,}000$).

Dimensionality Reduction and Transcriptional Landscape Visualization

Dimensionality reduction of the dataset to embed the samples in a two-dimensional landscape was performed using the principle component analysis (PCA) estimation routine in the package pcaMethods in R. Gene expression values from all control LLM and control PHx samples were subjected to PCA. The first four principle components, capturing nearly 46% of the variability in the data, were selected as an orthonormal basis on to which the expression values ethanol LLM and ethanol PHx samples were projected yielding a four-dimensional dataset for all samples. The dimensionality of the dataset was further reduced using the t-SNE method[30] implemented in R (package tsne). Application of the t-SNE method on sample scores and projections on the four-dimensional orthonormal basis retained after PCA yielded a two-dimensional embedding of all samples in the data.

RESULTS

We obtained a novel single-cell data set on the expression of 84 genes, each measured in 233 individual hepatocytes obtained using laser capture microdissection (LCM) from four rat livers (two chronic ethanol diet and two pair-fed control diet) at two time points: LLM (0 h, baseline) and PHx (24 h). We collected single hepatocytes from the midlobular region in order to focus on the variability of gene expression that is not dominated by the known large differences between the pericentral and

periportal regions (Fig. 1A workflow schematic). Images demonstrating single-cell lifts from liver sections using LCM are shown in Figure 1B. Single-cell gene expression was assayed via high-throughput real-time PCR to yield a large-scale data set containing 19,572 individual qRT-PCR measurements. We measured the expression of a panel of genes corresponding to metabolic functions, growth factor signaling, transcriptional regulation, cell proliferation, apoptosis, and xenobiotic clearance (see Table 1 for relevant GO Slim ontologies). Quality control analysis demonstrated that our workflow has minimal cross-cellular contamination (Fig. 2) and is sensitive enough to detect gene expression over six orders of magnitude with minimal technical variability in repeated measures (Fig. 2). This is consistent with our previous results that the typical biological variation at single-cell scale is significantly larger than well-controlled technical noise[5,31]. The raw data were subjected to multiple quality control tests to filter for high-quality data for the subsequent analysis (see Materials and Methods). Twenty-nine percent of the data were discarded by quality control analysis for failed reactions, improper sample loading, or poor signal quality. The missing values in the data set were imputed using a k-nearest neighbor approach[27]. Analysis of gene expression stability using GeNorm[25,26] suggested the median gene expression as the most robust factor for normalizing the data (Fig. 2C). Accordingly, we normalized the data to the median expression within each cell, followed by median subtraction across single cells. The quality control, imputation, and normalization steps yielded a data matrix of 84 genes and 233 single-cell samples that was considered in subsequent analysis (Fig. 1C). We did not see evidence for substantial animal-to-animal differences in our dataset (see Table 2).

Gene Expression Variability and Modularity in Single Hepatocytes In Vivo

Gene expression varied widely across individual hepatocytes. A subset of the data comprising 90% of single cells and all the genes showed expression over an 84-fold range, consistent with typical single-cell gene expression results in other tissues[5,31]. Although the overall gene expression was highly variable, a subset of genes showed statistically significant differences due to chronic ethanol intake, PHx, and a combination of the two perturbations (see the two-factor ANOVA results highlighted in Fig. 1C). For instance, the number of single hepatocytes that expressed Ccnd1 was higher after PHx, and this was also reflected as an increase in the mean Ccnd1 expression between PHx and baseline groups (Fig. 1D). We observed an elevated expression of one of the aldehyde dehydrogenase isoforms (Aldh7a1) as well as one of the cytochrome p450 genes (Cyp2a1) in the ethanol LLM samples. Notably, the mean expression differences of the statistically significant genes were in the one- to twofold range, much lower than the overall range of single-cell

Table 1. Ontological Classification of Genes Included in This Study

GOSlim GOA Accession	GOSlim GOA Description	Genes
GO:0000988	Transcription factor activity, protein binding	Sirt1
GO:0001071	Nucleic acid-binding transcription factor activity	Cebpg, Hnf4a, Nr4a1, Ppara, Srebp2, Stat5a
GO:0005975	Carbohydrate metabolic process	Dlat, G6pd, Gapdh, Gusb, Pck1, Pfkfb1, Pklr
GO:0006091	Generation of precursor metabolites and energy	Idh3a, Idh3b
GO:0006520	Cellular amino acid metabolic process	Asl, Glul, Got1, Oat
GO:0006629	lipid metabolic process	Acly, Acox1, Acox3, Apoa4, Cpt1, Fabp1, Fasn, Fatp5, Hmgcs1
GO:0006950	Response to stress	Fos, Hif1a, Il1r1, Il6r, Irak1, Jun, Ldha, Nfkb2, p38Mapk, Pdk1, Socs3, Stat3, Tnfa, Tnfr1
GO:0007049	Cell cycle	Ccnd1
GO:0007165	Signal transduction	Vegfa
GO:0008219	Cell death	Bax, Casp12, Casp3, Casp8, Fadd, Igf1r
GO:0008283	Cell proliferation	Ang1, Pdgfa, Smad1, Smad2, Tgfbr1, Tgfbr2, Tgif
GO:0008289	Lipid binding	Alb, Rxra
GO:0016491	Oxidoreductase activity	Adh1, Aldh1a1, Aldh1b1, Aldh2, Aldh7a1, Ch25h, Cyp1a1, Cyp1a2, Cyp2a1, Cyp2e1, Cyp3a1, Cyp4a1
GO:0016746	Transferase activity, transferring acyl groups	Cpt2, Lrat
GO:0030154	Cell differentiation	Bcl2l1, cMet, Smad3, Smad7
GO:0030198	Extracellular matrix organization	Gfap
GO:0032182	Ubiquitin-like protein binding	Ubqln1
GO:0044281	Small molecule metabolic process	Erlin2
GO:0065003	Macromolecular complex assembly	Tbp
GO:0071941	Nitrogen cycle metabolic process	Arg1, Ass1

Table 2. Gene Expression Differences Between Animals Identified Using Two-Factor ANOVA (Time point: LLM or PHx)

	Control			
	LLM		PHx	
Gene	Tukey HSD (Animal 5 − Animal 1)	*p* Value (BH Corrected)	Tukey HSD (Animal 5 − Animal 1)	*p* Value (BH Corrected)
Acly	−1.432	0.098	−0.586	1
Acox1	−0.809	0.892	−0.692	1
Acox3	0.024	1	−0.815	0.562
Adh1	0.908	0.762	1.918	0.068
Alb	−2.013	0.009	−0.727	0.954
Aldh1a1	2.477	0.039	1.536	0.562
Aldh1b1	0.9	0.95	−0.263	1
Aldh2	−0.727	0.599	−0.152	1
Aldh7a1	−0.285	1	0.004	1
Ang1	−0.305	1	0.399	1
Apoa4	−0.645	0.338	−0.337	1
Arg1	−0.3	1	−0.972	0.437
Asl	1.21	0.727	−0.049	1
Ass1	−1.953	0.039	0.006	1
Bax	0.725	0.727	1.399	0.098
Bcl2l1	0.373	1	0.055	1
Casp12	1.032	0.436	−1.144	0.44
Casp3	−0.405	1	−0.354	1
Casp8	−0.307	1	−0.879	0.608
Ccnd1	−0.318	1	−0.976	1
Cebpg	1.118	0.106	−0.446	1
Ch25h	−0.153	1	−0.454	1
cMet	1.708	0.159	2.018	0.112
Cpt1	0.218	1	−0.404	1
Cpt2	0.551	1	−0.377	1
Cyp1a1	−1.303	0.616	0.872	1
Cyp1a2	−1.947	0.027	−0.452	1
Cyp2a1	0.089	1	0.433	1
Cyp2e1	0.573	1	−0.298	1
Cyp3a1	0.38	1	0.063	1
Cyp4a1	1.089	0.322	1.5	0.106
Dlat	0.149	1	0.087	1
Erlin2	1.911	0.159	0.437	1
Fabp1	−1.247	0.172	1.01	0.599
Fadd	0.429	1	−0.713	0.902
Fasn	−0.673	0.503	−0.519	0.954
Fatp5	0.212	1	0.42	1
Fos	0.142	1	0.934	1
G6pd	−0.098	1	0.064	1
Gapdh	0.104	1	−1.132	0.056
Gfap	−0.341	1	−0.078	1
Glul	0.408	1	−0.57	0.95
Got1	0	1	0.16	1
Gusb	0.421	1	0.319	1
Hif1a	0.825	0.608	−0.995	0.514
Hmgcs1	1.345	0.406	1.24	0.637
Hnf4a	−0.297	1	−0.515	0.902
Idh3a	−1.245	0.068	−0.3	1
Idh3b	−0.367	1	−0.691	0.892
Igf1r	−0.134	1	−0.194	1

(*continued*)

Table 2. (Continued)

	Control			
	LLM		PHx	
Gene	Tukey HSD (Animal 5 − Animal 1)	*p* Value (BH Corrected)	Tukey HSD (Animal 5 − Animal 1)	*p* Value (BH Corrected)
Il1r1	1.872	0.095	0.672	1
Il6r	−0.147	1	−0.683	0.727
Irak1	1.344	0.436	1.495	0.436
Jun	−0.072	1	−0.889	0.95
Ldha	0.386	1	−0.609	0.822
Lrat	0.247	1	−0.332	1
Nfkb2	1.314	0.011	−0.546	0.902
Nr4a1	0.702	1	0.058	1
Oat	1.129	0.382	0.656	1
p38Mapk	0.895	0.166	−0.209	1
Pck1	0.006	1	−0.089	1
Pdgfa	2.038	0.128	0.113	1
Pdk1	1.451	0.159	2.009	0.048
Pfkfb1	−0.482	1	0.039	1
Pklr	−1.684	0.016	−0.553	1
Ppara	1.805	0.095	1.801	0.159
Rxra	−0.855	0.338	0.03	1
Sirt1	2.359	0.039	1.444	0.599
Smad1	0.547	0.95	−0.604	0.954
Smad2	1.267	0.608	1.45	0.599
Smad3	0.658	0.436	0.251	1
Smad7	0.429	1	−0.718	0.892
Socs3	0.087	1	−0.797	0.382
Srebp2	−0.405	1	0.58	1
Stat3	0.981	0.166	0.946	0.368
Stat5a	1.254	0.159	0.573	1
Tbp	1.551	0.214	1.062	0.892
Tgfbr1	0.66	0.724	−0.451	1
Tgfbr2	−0.594	1	−0.129	1
Tgif	0.207	1	−0.681	1
Tnfa	1.866	0.011	1.757	0.044
Tnfr1	0.491	1	−0.012	1
Ubqln1	−0.325	1	−0.713	0.503
Vegfa	−1.781	0.044	−0.708	1

	Ethanol			
	LLM		PHx	
Gene	Tukey HSD (Animal 6 − Animal 2)	*p* Value (BH Corrected)	Tukey HSD (Animal 6 − Animal 2)	*p* Value (BH Corrected)
Acly	0.009	1	0.332	1
Acox1	0.307	1	−0.645	1
Acox3	1.079	0.76	0.31	1
Adh1	2.246	0.003	0.584	1
Alb	1.376	0.356	0.41	1
Aldh1a1	1.042	1	2.018	0.278
Aldh1b1	1.152	1	−0.435	1
Aldh2	−0.121	1	1.271	0.327
Aldh7a1	−0.761	1	0.445	1
Ang1	−0.335	1	0.053	1

(*continued*)

Table 2. (Continued)

	Ethanol			
	LLM		PHx	
Gene	Tukey HSD (Animal 6 − Animal 2)	*p* Value (BH Corrected)	Tukey HSD (Animal 6 − Animal 2)	*p* Value (BH Corrected)
Apoa4	0.152	1	−0.322	1
Arg1	−0.145	1	1.118	0.561
Asl	−1.19	1	1.525	0.76
Ass1	1.141	0.327	0.294	1
Bax	0.933	1	0.371	1
Bcl2l1	−1.022	0.233	−1.394	0.02
Casp12	−0.199	1	0.724	1
Casp3	−0.761	1	0.11	1
Casp8	−0.637	1	−1.268	0.114
Ccnd1	1.41	0.76	−0.185	1
Cebpg	0.626	1	−0.266	1
Ch25h	−0.753	0.993	−0.659	1
cMet	1.85	0.233	1.418	0.641
Cpt1	−0.266	1	−0.253	1
Cpt2	−0.836	1	−0.319	1
Cyp1a1	2.045	0.327	1.125	1
Cyp1a2	−0.09	1	−1.294	0.327
Cyp2a1	1.51	0.093	−0.372	1
Cyp2e1	−0.828	1	−1.15	0.897
Cyp3a1	−0.039	1	−1.091	0.803
Cyp4a1	0.379	1	0.551	1
Dlat	−0.883	0.561	−0.577	1
Erlin2	1.84	0.327	1.388	0.803
Fabp1	1.657	0.22	−1.407	0.35
Fadd	−0.471	1	−1.573	0.006
Fasn	0.057	1	0.504	1
Fatp5	0.442	1	0.111	1
Fos	0.923	1	0.833	1
G6pd	−1.546	0.233	−0.303	1
Gapdh	−0.105	1	−0.974	0.249
Gfap	−0.761	1	−1.07	0.631
Glul	−1.056	0.327	0.297	1
Got1	−0.224	1	2.047	0.01
Gusb	−0.905	0.645	−0.152	1
Hif1a	−0.347	1	−0.317	1
Hmgcs1	2.823	0.004	3.059	0.003
Hnf4a	0.3	1	−0.729	1
Idh3a	−0.325	1	0.221	1
Idh3b	−0.844	0.76	−0.032	1
Igf1r	−1.158	0.124	−1.039	0.233
Il1r1	1.544	0.806	0.591	1
Il6r	−0.588	1	0.004	1
Irak1	0.184	1	2.287	0.114
Jun	−0.318	1	−0.423	1
Ldha	−0.593	1	0.231	1
Lrat	−1.018	0.561	−1.119	0.377
Nfkb2	0.483	1	0.817	0.993
Nr4a1	0.59	1	0.292	1
Oat	−0.7	1	0.904	1
p38Mapk	−0.535	1	0.324	1
Pck1	1.548	0.22	1.495	0.233

(*continued*)

Table 2. (Continued)

	Ethanol			
	LLM		PHx	
Gene	Tukey HSD (Animal 6 − Animal 2)	*p* Value (BH Corrected)	Tukey HSD (Animal 6 − Animal 2)	*p* Value (BH Corrected)
Pdgfa	0.57	1	−0.058	1
Pdk1	0.355	1	1.002	0.897
Pfkfb1	0.221	1	0.036	1
Pklr	−0.977	0.981	−0.75	1
Ppara	2.845	0.005	0.994	1
Rxra	0.767	0.993	0.041	1
Sirt1	1.484	0.803	0.551	1
Smad1	−0.581	1	−0.551	1
Smad2	0.632	1	3.272	0.004
Smad3	0.036	1	0.326	1
Smas7	−1.15	0.312	−1.28	0.22
Socs3	−0.508	1	−0.663	1
Srebp2	0.168	1	0.992	1
Stat3	−0.438	1	−0.018	1
Stat5a	0.54	1	−0.302	1
Tbp	0.854	1	1.518	0.76
Tgfbr1	−0.683	0.981	0.014	1
Tgfbr2	−0.183	1	0.151	1
Tgif	−0.292	1	0.185	1
Tnfa	0.719	1	0.733	1
Tnfr1	−0.035	1	0.962	1
Ubqln1	0.076	1	0.185	1
Vegfa	0.3	1	0.573	1

Normalized expression values from the two animals (animals 1 and 5) subjected to the control diet as well as the two animals subjected to the ethanol diet (animals 2 and 6). Post hoc analysis was performed using the Tukey HSD test with =0.05. Only a small subset of genes showed differences between animals within diets. LLM, left lateral and medial lobes; PHx, partial hepatectomy.

gene expression. Hierarchical clustering yielded several modules of correlated gene expression that separated hepatocytes into distinct transcriptional states. We analyzed the change in proportion and composition of these transcriptional states across multiple experimental conditions, as described in the following sections.

Hepatocytes Are Distributed Along Multiple Gene Expression States In Vivo at Baseline. We performed hierarchical clustering analysis to separate the control LLM samples into seven clusters exhibiting distinct gene expression profiles (Fig. 4A). These clusters were characterized by correlated expression patterns of three distinct subgroups of genes. Whereas gene group 3 (Fig. 4A) comprised primarily of metabolism-related genes, gene groups 1 and 2 consisted of a mixture of genes corresponding to a range of cellular functions such as cytokine reception, metabolic regulation, immediate early response, etc.

We analyzed the molecular states of hepatocyte clusters as represented by the combinatorial expression profile of select functionally relevant genes. The set of classifying genes was selected based on the experimental perturbations of chronic ethanol consumption and PHx. The mitogenic and angiogenic response of hepatocytes was captured by the expression of Ccnd1, Vegfa, and Ang1[32–34]. Additionally, we included immediate early response genes (Fos, Jun) as well as primed state markers (Il6r, Stat3, Socs3, Tnfr1, Nfkb2, and c-Met). Using the chosen set of classifying genes, we were able to identify four different hepatocyte subpopulations as follows. Two of the seven hepatocyte clusters (Fig. 4A, State 1) showed low-to-moderate expression of metabolic genes, immediate early genes, priming phase markers, as well as mitogenic response markers. These clusters, which comprise 36% of the control LLM samples, are likely characterized as representing a baseline quiescent state. Sample clusters in State 2 (51% of the control LLM samples) exhibited elevated expression of priming phase markers and immediate early genes compared to State 1, but low expression of mitogenic/angiogenic response and metabolic genes. State 3 (10% of the control LLM samples) showed high expression of primed phase markers as well as mitogenic/angiogenic response genes (Ccnd1 and Ang1). A small proportion of cells (State 4, 3% of the control LLM samples) showed low levels of primed state markers but higher levels of mitogenic/angiogenic response genes Ccnd1, Vegfa, and Ang1.

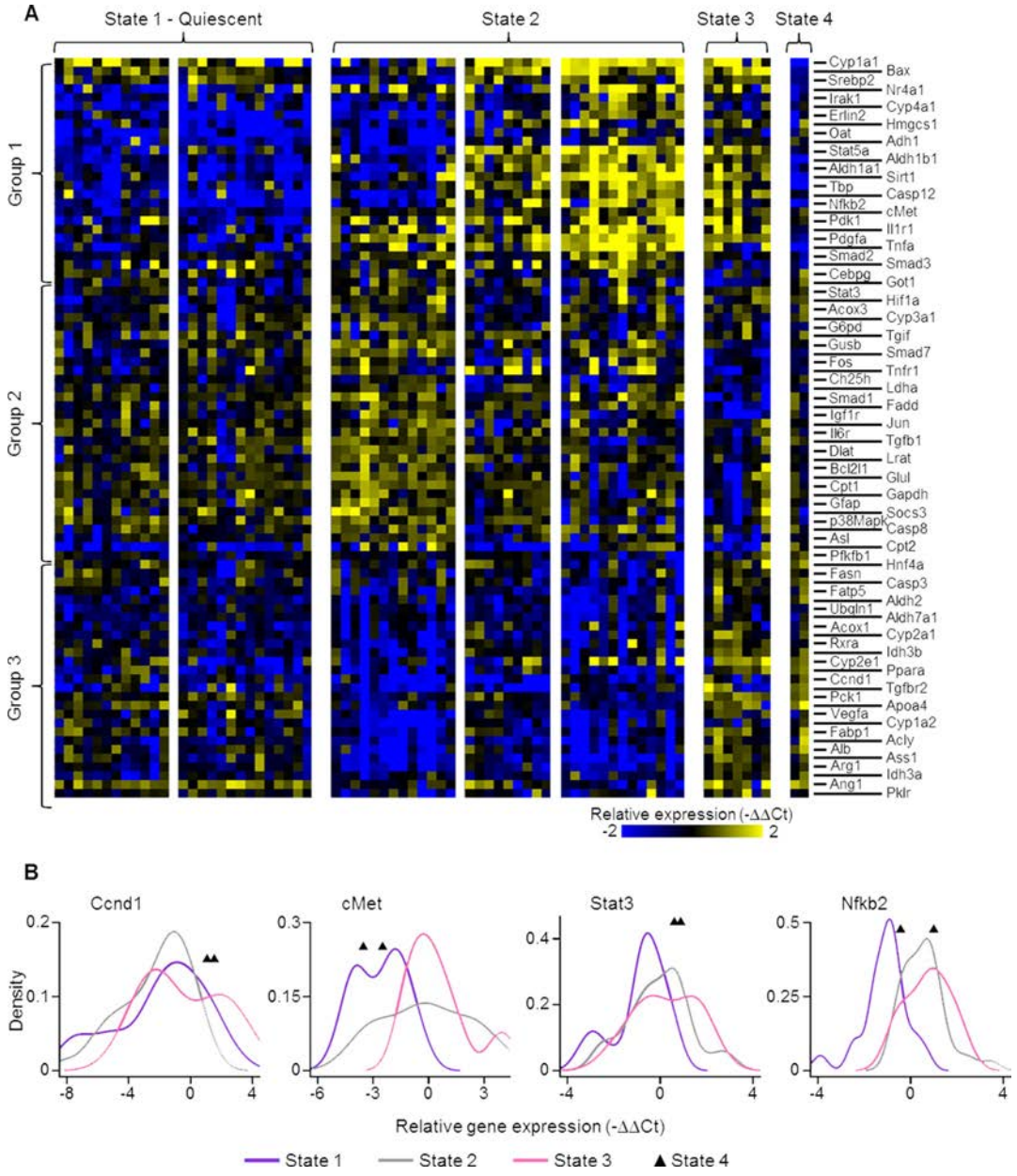

Figure 4. Control LLM hepatocytes reside across four different molecular states. (A) Pearson's correlation-based hierarchical clusters of samples and genes. Seven-sample and three-gene clusters are shown. The seven-sample clusters are used as templates for template matching throughout the rest of the analysis. One of the four hepatocyte states could likely be the quiescent state owing to low expression of primed phase and replication/angiogenesis marker genes. (B) State 1 likely contains hepatocytes in the quiescent state. Samples residing in State 1 exhibit low expression of Ccnd1 (replication phase marker), cMet (HGF receptor), and Stat3 and Nfkb2 (primed phase markers).

PHx Shifts Hepatocyte Molecular States Toward the Replicating Phenotype. Although the systemic and local signals that lead to liver regeneration are activated within seconds of PHx and last up to a week, the 24-h mark is a key time point in the case of rat liver regeneration characterized by the strongest peak in DNA synthesis, coinciding with a peak in hepatocyte replication[15]. Our previous transcriptomic analysis of whole tissue revealed significant differences in gene expression between ethanol and control groups at the 24-h time point[13]. We therefore sought to characterize the hepatocyte states 24 h after PHx to enable comparison across the ethanol and isocaloric control groups. We used a similar template match-based approach to evaluate the molecular signatures of the hepatocyte subpopulations 24 h after liver resection in control animals (Fig. 5A). Expression profiles of 60%

of the control PHx hepatocytes directly matched the control LLM clusters. The unmatched control PHx samples (Fig. 5A) were clustered separately and reclassified into the four subpopulations identified in control LLM samples based on hierarchical clustering of gene medians of all clusters.

Hepatocytes from control PHx samples reside in the four subpopulations identified in control LLM samples. The distribution of control PHx samples between the four subpopulations revealed significant shifts in sample proportions compared to control LLM (chi-square $p < 0.001$) (Fig. 5A and B; see Tables 3 and 4). Only 3% of control PHx samples show expression profiles similar to the quiescent subpopulation, a drastic decrease in proportions from 36% in control LLM samples. The fraction of control PHx hepatocytes also decreased substantially in State 2 (from 50% to 25%) but only slightly in State 3 (from 9% to 7%) compared to control LLM. The majority (62%) of the control PHx hepatocytes were classified in State 4, while the control baseline had only 3% of hepatocytes in this subpopulation.

State 4 control PHx samples showed elevated mitogenic/angiogenic response gene expression (Ccnd1, Ang1, and Vegfa), similar to control LLM samples. In the context of regenerating liver, this subpopulation could represent the hepatocyte replication state. This observation was consistent with previously published results, where liver regeneration peaks at 24 h after PHx in rats[18,35,36]. Furthermore, the fraction of replicating hepatocytes at 24 h after resection was consistent with previous findings on BrdU incorporation or Ki-67 protein expression[37]. Similar to control LLM, the control PHx hepatocytes lying in State 2 showed elevated expression of priming markers. We could now identify State 2 as a priming subpopulation in response to the regenerative stimulus generated due to partial hepatectomy. State 3 hepatocytes from control LLM and control PHx groups showed a combinatorial expression of priming and replication genes. In the context of hepatic regeneration, we could now define this state as a transition between priming and replicating hepatocyte subpopulations.

The metabolic gene expression of control PHx hepatocytes was consistent with that observed in whole tissue liver regeneration studies. We observed an increase in expression of gluconeogenesis and fatty acid -oxidation genes (Pck1, Acox1, Ppara, and Rxr) and a decrease in glycolytic gene (Pklr) in control PHx samples (Fig. 5C), as reported previously[38]. Furthermore, our data indicated an increase in fatty acid trafficking (elevated levels of Fatp5 and Fabp1), a phenomenon previously observed in regenerating livers[39].

In addition to a high proportion of samples residing in the replicating subpopulation, control PHx samples showed elevated expression of mitogenic/angiogenic markers Ccnd1, Ang1, and Vegfa compared to control baseline samples in all subpopulations except quiescent (Fig. 5D). Expression of Pklr, a glycolytic gene, was suppressed in all subpopulations in control PHx hepatocytes suggesting a shift from glycolytic to gluconeogenic carbohydrate metabolism. Furthermore, we observed increased expression of Ppara and Fabp1 in control PHx samples compared to control LLM samples in the primed state. These observations could indicate induction of downstream fatty acid -oxidation targets of Ppara and higher activity of fatty acid trafficking by Fabp1 before the hepatocytes enter the cell cycle.

Consistent with expectation, our analysis pointed toward a large dissimilarity between hepatocytes in the proportion of hepatocytes existing in the four subpopulations before and after PHx. Control PHx hepatocytes preferentially occupy primed or replicating subpopulations. Furthermore, gene expression signatures of liver regeneration were readily recognizable at the single hepatocyte level in our data.

Chronic Ethanol Intake Alters the Distribution of Single Hepatocyte Subpopulation Distributions. We further employed our template matching approach to identify distribution of ethanol LLM samples between the four hepatocyte subpopulations (Fig. 6). Our analysis revealed that a large fraction of ethanol-adapted hepatocytes (77%) exhibit gene expression patterns similar to the subpopulations identified in control baseline samples, suggesting a high degree of adaptation to chronic ethanol feeding. The remaining 23% samples were separated into three new clusters (Fig. 6A). Hierarchical clustering of cluster medians post-template matching revealed that the gene expression profiles in the three new clusters held higher similarity with the primed-to-replicating transition subpopulation and the replicating subpopulation.

Although all control LLM subpopulations were observed in ethanol LLM hepatocytes as well, the proportions of ethanol-adapted hepatocytes belonging to these subpopulations vary significantly from the control baseline samples (chi-square $p = 0.003$) (see Tables 3 and 4). For instance, the proportion of ethanol LLM hepatocytes belonging to the quiescent subpopulation decreased compared to control baseline hepatocytes (from 36% in control LLM to 22% in ethanol LLM) (Fig. 6B). Similarly, the fraction of primed hepatocytes decreased from 51% to 36% in the ethanol LLM group compared to control LLM. By contrast, an increase was observed in the fraction of hepatocytes belonging to the primed-to-replicating transition state (22% in ethanol LLM vs. 10% in control LLM). The remaining ethanol LLM samples (20%) showed a high degree of similarity in gene expression to the replication subpopulation, a noticeable increase compared to only 3% of hepatocytes in the control LLM

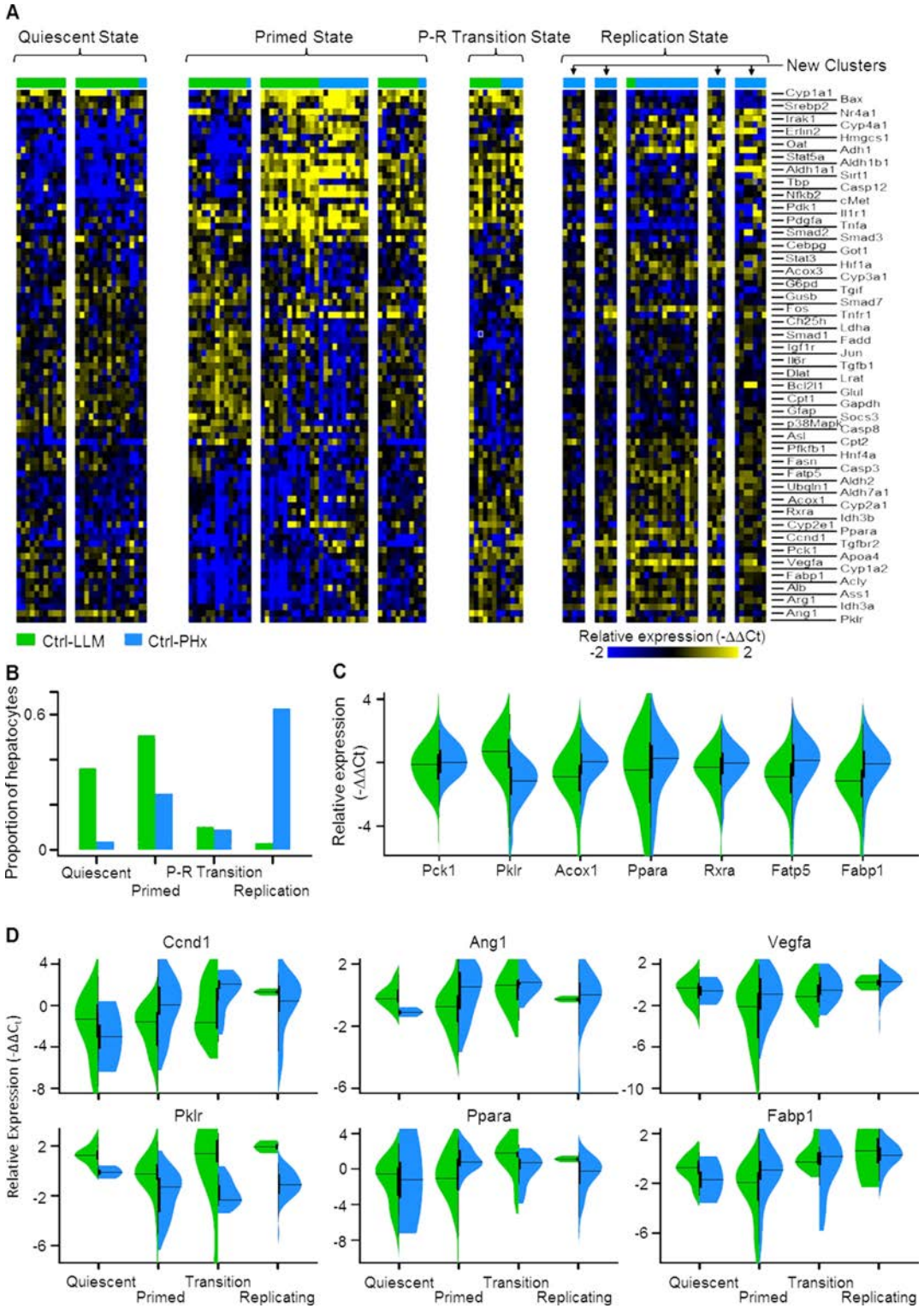
A
Quiescent State
Primed State
P-R Transition State
Replication State
New Clusters
Cyp1a1 Bax
Srebp2 Nr4a1
Irak1 Cyp4a1
Erlin2 Hmgcs1
Oat Adh1
Stat5a Aldh1b1
Aldh1a1 Sirt1
Tbp Casp12
Nfkb2 cMet
Pdk1 Il1r1
Pdgfa Tnfa
Smad2 Smad3
Cebpg Got1
Stat3 Hif1a
Acox3 Cyp3a1
G6pd Tgif
Gusb Smad7
Fos Tnfr1
Ch25h Ldha
Smad1 Fadd
Igf1r Jun
Il6r Tgfb1
Dlat Lrat
Bcl2l1 Glul
Cpt1 Gapdh
Gfap Socs3
p38Mapk Casp8
Asl Cpt2
Pfkfb1 Hnf4a
Fasn Casp3
Fatp5 Aldh2
Ubqln1 Aldh7a1
Acox1 Cyp2a1
Rxra Idh3b
Cyp2e1 Ppara
Ccnd1 Tgfbr2
Pck1 Apoa4
Vegfa Cyp1a2
Fabp1 Acly
Alb Ass1
Arg1 Idh3a
Ang1 Pklr
Ctrl-LLM
Ctrl-PHx
Relative expression (-ΔΔCt)
-2
2
B
Proportion of hepatocytes
0.6
0
Quiescent
Primed
P-R Transition
Replication
C
Relative expression (-ΔΔCt)
4
-4
Pck1
Pklr
Acox1
Ppara
Rxra
Fatp5
Fabp1
D
Ccnd1
Ang1
Vegfa
Pklr
Ppara
Fabp1
Relative Expression (-ΔΔCt)
Quiescent
Primed
Transition
Replicating

Table 3. Contingency Table Listing the Number of Hepatocytes From Each Condition in Every Subpopulation

	Quiescent	Primed	Transition	Replication
Control LLM	25	35	7	2
Control PHx	2	14	5	35
Ethanol LLM	12	20	12	11
Ethanol PHx	6	11	13	24

Table 4. Post Hoc *p* Values for Differences in Proportions of Hepatocytes Residing in Each Subpopulation Between Conditions

Comparison	Raw *p* Value	Adj. *p* Value
Control LLM versus control PHx	0	0
Control LLM versus ethanol LLM	0.002	0.003
Control LLM versus ethanol PHx	0	0
Control PHx versus ethanol LLM	0	1E-04
Control PHx versus ethanol PHx	0.0474	0.047
Ethanol LLM versus ethanol PHx	0.0236	0.028

samples. Overall we observed a lower proportion of ethanol LLM samples in the earlier subpopulations (quiescent and primed) compared to the control LLM hepatocytes.

We further examined the effect of chronic ethanol adaptation by comparing the expression of alcohol clearance genes within each subpopulation compared to the controls. Alcohol clearance in the liver occurs through two major transcriptional modules: alcohol and aldehyde dehydrogenases, and cytochrome P450 (CYP) family genes. Alcohol dehydrogenase (ADH) is responsible for oxidizing most of the ethanol passing through the liver in the circulation with cytochrome P40 2E1 (Cyp2e1) contributing a variable proportion of ethanol metabolism, particularly at higher blood alcohol levels[40]. Both metabolic pathways result in the formation of acetaldehyde, which is cleared predominantly through the mitochondrial aldehyde dehydrogenase isoform 2 (Aldh2). We observed an increase in Adh1 gene expression in ethanol LLM hepatocytes in all the subpopulations when compared to the control LLM. Our data suggested moderately increased expression of Aldh2 compared to control samples in the quiescent, primed, and replicating subpopulations but not the transition subpopulation (Fig. 6C). Cyp2e1 is expected to exhibit higher activity under chronic ethanol adaptation in part due to protein stabilization by ethanol[41]. We observed higher expression of Cyp2e1 in ethanol LLM samples compared to control LLM in the quiescent and primed subpopulations but not in the transition and replicating subpopulations.

We compared the expression of lipid metabolism and transport-related genes between control and ethanol baseline hepatocytes across all subpopulations. Our data indicated increased expression levels of Fasn as well as Fatp5 in ethanol LLM samples (Fig. 6D). In addition, expression of Fabp1, which has been reported to suppress intracellular lipotoxicity in humans[42], was increased.

Chronic Ethanol Alters PHx-Induced Shifts Between Hepatocyte Subpopulations Toward an Overall Lower Regenerative State. Chronic alcohol-adapted livers exhibit delayed or insufficient liver regeneration after injury[22]. We sought to determine whether gene signatures for the suppressed regenerative response can be observed at the level of single hepatocyte population distributions in ethanol-adapted livers postresection. We employed our template match analysis to identify the shifts in molecular expression observed in chronic ethanol-adapted single hepatocytes 24-h postresection. As in previous sections, we used the control LLM sample cluster medians as templates for matching.

The results of our template match analysis are shown in Figure 7. Similar to the control PHx samples, only 40% of the ethanol PHx samples matched the control LLM templates. The unmatched samples were separated into three different clusters. Although similar fractions of control and ethanol PHx samples matched with the control LLM templates, the distribution of hepatocytes across the four subpopulations was different between these sample groups (chi-square $p = 0.047$) (Fig. 7B; see Tables 3 and 4). While control PHx samples exhibited a drastic increase in the fraction of hepatocytes in the replicating subpopulation, the increase in replicating ethanol PHx samples was much less pronounced. A higher fraction of ethanol PHx samples were in the quiescent and transition subpopulations compared to control PHx samples.

FACING PAGE

Figure 5. Control PHx samples reside primarily in the primed and replicating subpopulations. The primed state is characterized by high expression of priming phase markers, whereas the replication state is characterized by high expression of Ccnd1 and genes participating in angiogenesis (Ang1, Vegfa). (A) Distribution of control PHx samples (blue) across the molecular states identified in control LLM samples. The new states identified in control PHx samples exhibit gene expression profiles closest to the replicating state. (B) Control PHx hepatocytes (62.5%) reside in the replication state. In contrast, 2.9% control LLM samples reside in the replication state. (C) Elevated fatty acid/lipid metabolism and transport gene expression (Acox1, Rxra, Ppara, Fatp5, Fabp1) and decreased glycolytic gene expression (Pklr) compared to control LLM samples (green). (D) Subpopulation-specific comparisons suggest elevation in replication markers (Ccnd1, Ang1, and Vegfa) in control PHx sample in all subpopulations except quiescent. Pklr expression is suppressed in all subpopulations. Ppara and Fabp1 expression increases in control PHx samples in the primed state.

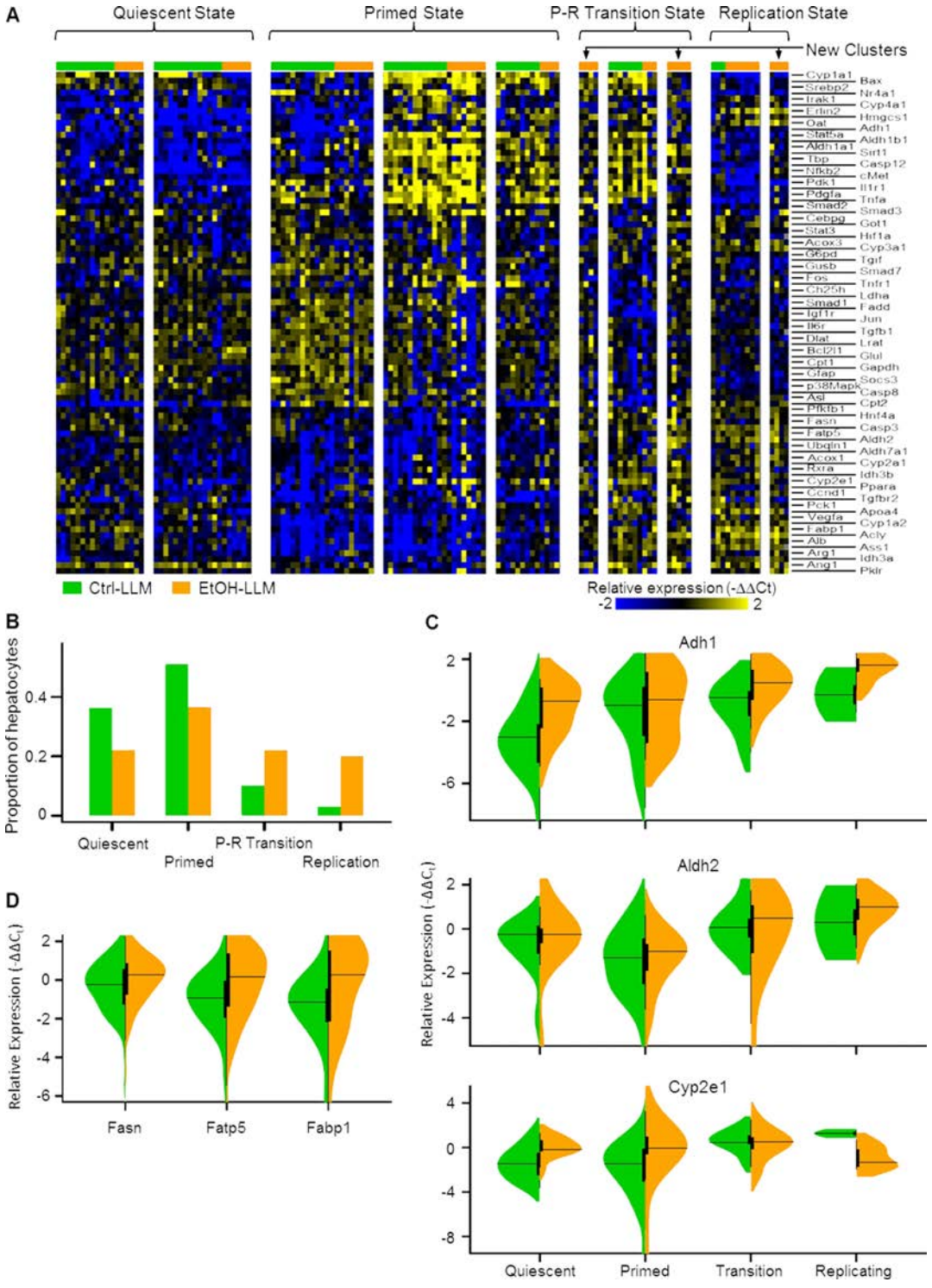

Figure 6. Distribution of ethanol LLM hepatocytes across molecular states is similar to control LLM samples. (A) Three new clusters identified in the ethanol LLM samples show gene expression profiles similar to the primed-to-replication transition state and the replication state. (B) Higher proportions of ethanol LLM samples reside in the transition and replication subpopulations compared to control LLM samples. (C) Elevated expression of alcohol and aldehyde metabolism genes in all molecular states in ethanol LLM samples compared to control LLM samples. (D) Dysregulated lipid metabolism and transport gene expression in ethanol LLM hepatocytes compared to control LLM hepatocytes.

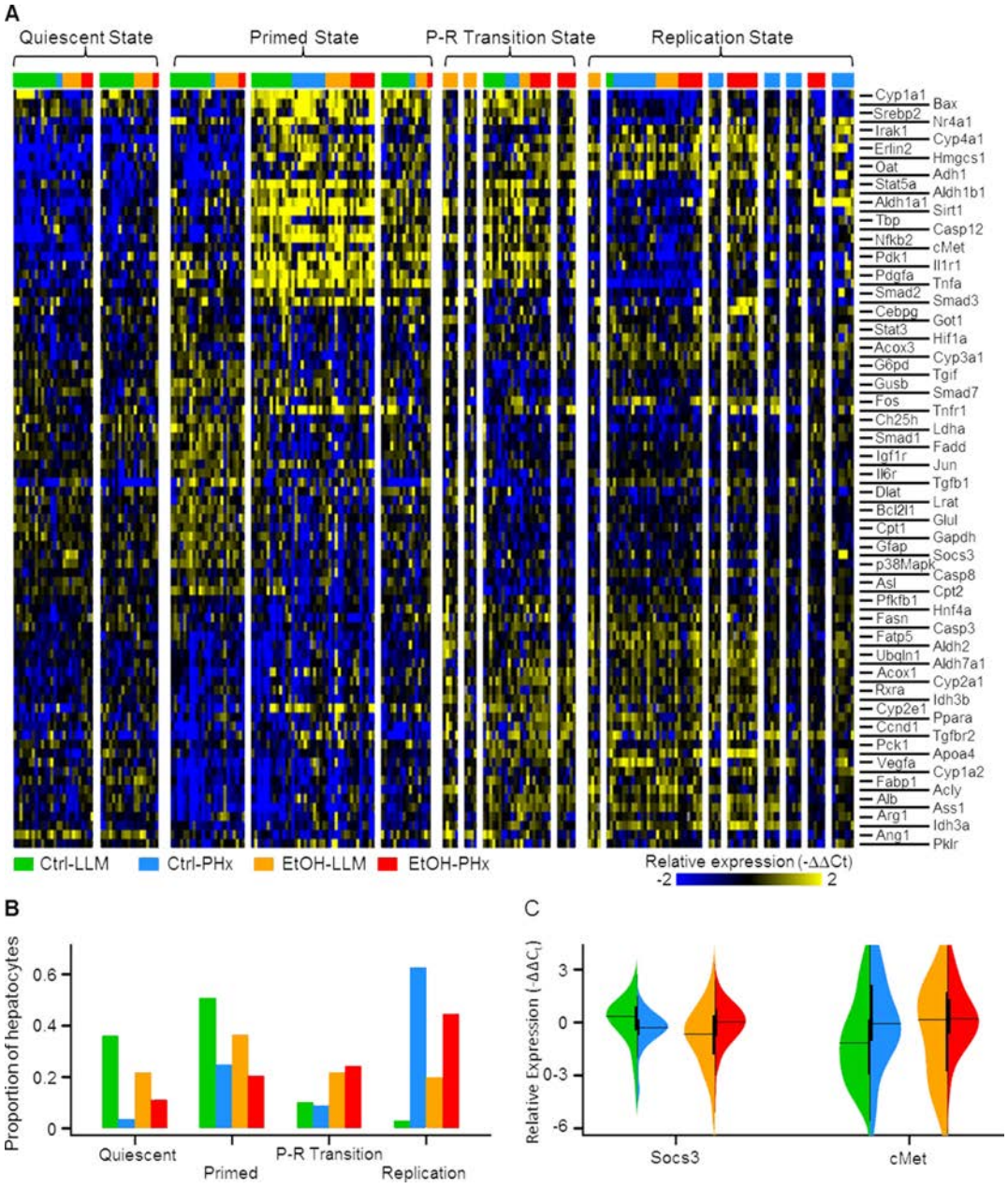

Figure 7. Distribution of hepatocytes from all conditions among the subpopulations identified in control LLM samples. (A) Samples from all conditions are distributed among all subpopulations, however, in different proportions. (B) PHx samples show increased fractions in the primed and replicating subpopulations in both diets. However, there is a higher fraction of control PHx samples in the replicating state compared to ethanol PHx. (C) Elevated Socs3 expression and unchanged cMet expression after PHx in ethanol PHx samples (red) compared to control PHx samples (blue) likely contribute to aberrant liver regeneration of rat livers adapted to chronic ethanol intake.

However, a similar fraction of control PHx and ethanol PHx hepatocytes occupied the primed state.

The higher fraction of ethanol PHx samples in the quiescent state suggested a suppressed priming response in alcohol-adapted livers, observable at the level of single hepatocytes. Sensitization of hepatocytes to ethanol-induced sustained cytokine signals has been reported previously, which could lead to their aberrant priming response after partial hepatectomy[43]. Studies in mice have reported that Socs3 deficiency improves liver regeneration by enhancing STAT3 and ERK activation[44]. Our data showed a decrease in Socs3 gene expression 24 h after PHx in the control case. However, we observed increased Socs3 gene expression 24 h after PHx in the

case of chronic ethanol-adapted livers. In addition, cMet expression increased after PHx in the case of control samples but not in ethanol samples. These observations point toward an underlying temporal dysregulation in expression of critical genes involved in hepatocyte priming in the case of chronic ethanol-adapted livers and could underlie the observed suppression of liver regeneration.

We further tested pSTAT3 and SOCS3 protein expression levels using Western blots and immunofluorescence to identify the differences in priming induced by PHx in control and chronic ethanol-adapted livers. Western blot results showed increased pSTAT3 and SOCS3 protein expression in control as well as ethanol groups 24 h post-PHx (Fig. 8A). Although the PHx-induced trends in

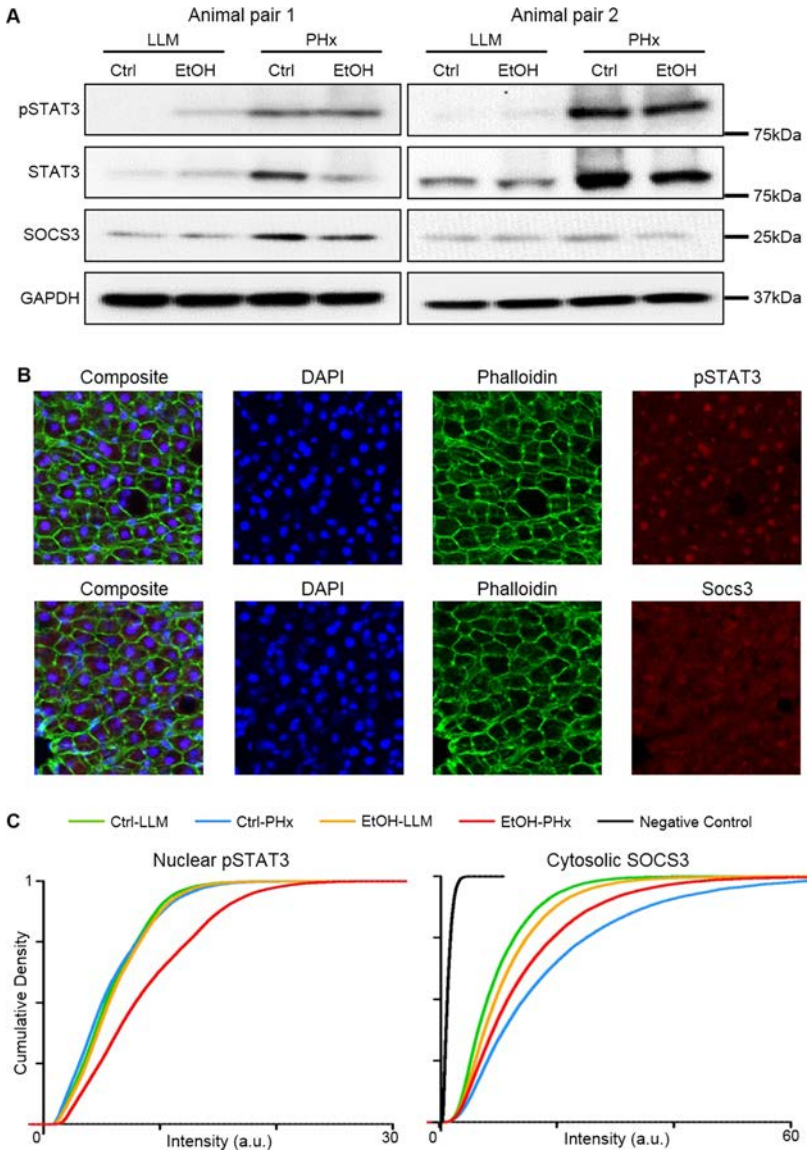

Figure 8. pSTAT3 protein exhibits higher nuclear localization in ethanol PHx hepatocytes. (A) Western blots for two animal pairs show increased pSTAT3 in both control and ethanol-adapted rat livers 24 h after PHx. PHx resulted in a blunted increase in SOCS3 levels for animal pair 2, compared to animal pair 1. (B) Examples of liver sections stained with DAPI, phalloidin and SOCS3 or pSTAT3 antibodies. The sections in the shown images were from a chronic ethanol-adapted animal 24 h after PHx. While pSTAT3 shows a high degree of colocalization with the nuclear DAPI signal, SOCS3 is more diffused throughout the cell. (C) Nuclear pSTAT3 localization is higher for ethanol PHx hepatocytes suggesting continued activity of priming signals. Distributions of cytosolic SOCS3 levels do not exhibit substantial differences between control and ethanol PHx. Fluorescent intensities in negative controls that lack the primary antibody are substantially lower than the true signal suggesting minimal nonspecific binding.

protein expression were similar at the whole tissue level in control and ethanol groups, the localization of pSTAT3 within hepatocytes was different at the 24-h time point (Fig. 8B and C). Quantitative analysis of protein immunofluorescence at the single-cell level revealed no changes in nuclear pSTAT3 protein in control PHx compared to that in control LLM. In contrast, the ethanol PHx group exhibited higher pSTAT3 localization in hepatocyte nuclei 24 h after resection compared to that in ethanol LLM. Our results showed a larger increase in cytosolic SOCS3 protein expression 24 h after PHx in the control group compared to ethanol. Increased pSTAT3 nuclear localization is consistent with higher Socs3 mRNA expression observed in our data (Fig. 7C). In conjunction, these results point toward a priming response in ethanol-adapted rat livers that is present even after 24 h post-PHx.

The effects of PHx on transcriptional states of hepatocytes at the 24-h time point in the control and ethanol groups can be visualized in a reduced dimensional space as shown in Figure 9. The transcriptional landscape consists of the four molecular states—quiescent, primed, transition, and replicating—as the "attractor" regions, the regions where hepatocytes tend to reside. A majority of control LLM samples occupy the quiescent and primed regions in the transcription landscape. PHx induces an overwhelming transition away from the quiescent attractor with a majority of control PHx hepatocytes residing in the replicating region of the transcriptional landscape. The regions of the transcriptional landscape occupied by the ethanol LLM samples overlap with the control LLM samples suggesting adaptation to chronic ethanol feeding. However, in the case of ethanol diet, hepatocytes seem to be distributed throughout the transcriptional landscape and continue to occupy similar regions after PHx. Existing evidence points toward sensitization of hepatocytes to high levels of cytokine signaling induced by chronic alcohol intake as one of the reasons for aberrant liver regeneration[43]. Although the difference in control and ethanol PHx sample proportions identified as quiescent was small, the higher proportion of ethanol PHx hepatocytes in the quiescent subpopulations compared to control PHx suggested a higher barrier for individual hepatocytes to transition away from quiescence. Notably, this effect was observable at the single-cell scale. The existence of small fractions of control and ethanol LLM samples in the regions of the transcriptional landscape occupied predominantly by replicating subpopulation in these sample groups could point toward tissue renewal rather than a regenerative response. Consistent with expectation, we observed higher tissue renewal response in ethanol baseline samples possibly caused due to alcohol metabolism intermediates and/or elevated cytokine levels mediating cell injury[45].

Ethanol Shifts Priming Response During Early Stages After PHx

Previous studies have demonstrated that suppressed liver regeneration due to adaptation to chronic ethanol intake in rats may be driven by events within the first few hours after PHx, before the 24-h peak of DNA synthesis. For instance, the expression of immediate early response genes at 1 h and 6 h after PHx is significantly different between control and ethanol-adapted rat liver[13]. In addition, binding profiles of NF- B also showed significant changes between control and ethanol-adapted rat liver at 1 h and 6 h after PHx[46]. In this work, we observed increased Socs3 gene expression (Fig. 7C) consistent

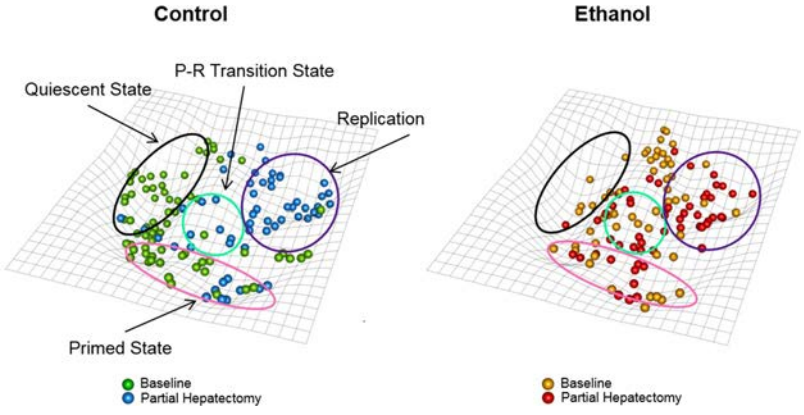

Figure 9. Adaptation to chronic ethanol intake causes suppressed shifts in molecular states of single hepatocytes after PHx. Control LLM and PHx hepatocytes occupy distinct regions within the transcriptional landscape with LLM samples residing predominantly in the quiescent and primed states, whereas the PHx samples reside predominantly in the primed-to-replication transition and replication states. In contrast, regions within the transcriptional landscape occupied by ethanol PHx samples show a higher overlap with those that contain ethanol LLM samples.

with increased nuclear pSTAT3 localization (Fig. 8C) at 24 h after PHx in the ethanol-adapted rat liver. Based on these results, we asked the question whether the pSTAT3 protein localization and Socs3 gene expression profiles at 24 h represent an overall temporal delay or a decoupling of the priming response and downstream cell cycle events in ethanol-adapted rat hepatocytes. We compared nuclear localization of pSTAT3 in control and ethanol groups at baseline and 6 h after PHx using immunofluorescence (Fig. 10). Our results showed that at 6 h after PHx, there is an increased nuclear localization of pSTAT3 in control samples. However, at 6 h post-PHx, the ethanol group did not show a substantial increase in nuclear pSTAT3 localization compared to the baseline, suggesting a reduction in hepatocyte priming in the early stages of regeneration in the ethanol-adapted rat liver, consistent with previous studies on whole tissue transcriptomic and genome-wide transcription factor binding[13,45]. Our results indicate that these trends are reversed 24 h after PHx, where there is increased nuclear pSTAT3 protein localization in ethanol PHx samples compared to baseline, but no change between control baseline and PHx samples (Fig. 8C). Such a delayed but sustained priming likely contributes toward the observed increase in the proportions of hepatocytes in quiescent and transition subpopulations at 24 h in the ethanol group compared to control.

DISCUSSION

In this study, we acquired a novel data set containing expression profiles of 84 genes from 233 individual hepatocytes residing in the midlobular region. Our results indicated that the effects of chronic ethanol exposure on liver regeneration are manifested in changes in the proportion of hepatocytes residing in baseline molecular states. These shifts in cell state proportions likely extrapolate to altered regenerative capacity of the liver.

Gene expression variability at the single-cell scale, as observed in our data, is now a widely recognized feature of tissues under homeostatic conditions. However, mounting a robust repair response to acute stimuli such as tissue injury requires a transient and potentially synchronized convergence of molecular states of individual cells toward a trajectory of molecular states leading to functional repair. Intercellular interactions mediated by local microenvironment modulation and/or direct molecular exchange are thought to play an important role in generating a concerted cellular response. Although intercellular communication can possibly override cellular variability at short time scales[47], effects on intracellular gene expression would require more precise regulation over longer time frames. Despite the intrinsic variability and microenvironmental effects, we observed modules of coexpressed genes within the focused gene set examined in this study, suggesting the existence of a set of "attractor cell states" in the liver following injury. Such attractor states are commonly observed across biological systems, particularly in the developmental context of lineage-specific differentiation, as well as in the immune system and highly organized tissue such as thebrain[5,48,49].

The current study was aimed at characterizing the distribution of the transcriptional states of hepatocytes in the liver during response to PHx. Our experimental design prioritized obtaining several single cells in order to have a reliable estimate of the transcriptional states. Considering the limited throughput of the laser capture microdissection-based approach to obtain single-cell samples, it was impractical to extend the design beyond two animals per condition (four conditions). We note that emerging technologies

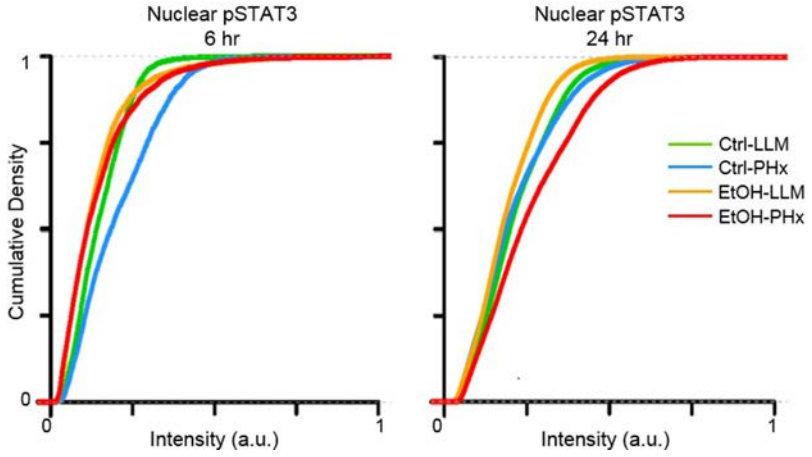

Figure 10. Six-hour versus 24-h nuclear pSTAT3 localization suggests dysregulated priming in chronic ethanol-fed rat livers after PHx. Nuclear pSTAT3 localization increases 6 h after PHx in control livers, but not in the ethanol-adapted livers. In contrast, nuclear pSTAT3 localization is elevated in ethanol livers 24 h after PHx, which is absent in control livers. The intensities were scale normalized for comparison between time points.

based on dissociated cells provide a fruitful path forward to obtain transcriptomic data from hundreds to low thousands of single cells, and could be extended to consider a larger set of individual animals for replicability. Such a data set would enable animal-to-animal comparisons in addition to diet and time point differences during liver regeneration. Additionally, we focused on a subset of 84 functionally relevant genes. Nevertheless, we note that even when considering the whole transcriptome, only a small fraction of transcripts (in the low hundreds) contributes to the classification of single-cell states, as not all transcripts are distinct in expression between the cell states[1,2] (i.e., the functional characterization of molecular states is determined by the subset of the transcriptome that is relevant to a specific biological context). Our study follows successful adaptation of focused gene expression studies in context-specific characterization of single-cell molecular states reported previously, for example, in the developmental context, brain, and colon[50–52].

In addition to the three canonical hepatocyte subpopulations—quiescent, primed, and replicating—we observed a fourth subpopulation that we classified as a primed-to-replicating transition state. Hepatocytes in this subpopulation are characterized by expression of primed state markers as well as mitogen response markers. The higher proportion of ethanol PHx samples (24%) compared to control PHx samples (8%) in the primed-to-replicating transition subpopulation suggested that in addition to hepatocyte sensitization and a slower priming response, progression of hepatocytes through the cell cycle itself is slower, contributing toward a suppression of liver regeneration. The recent emergence of advanced imaging techniques can provide further insight into transition rates of hepatocytes through the cell cycle in control and chronic ethanol-adapted cases[53]. Interestingly, a generalized prolongation or arrest of cell cycle progression has previously been observed in vitro due to chronic acetaldehyde treatment but not chronic ethanol treatment[54,55].

The results of our study indicate that an increase in tissue cytokine levels, subsequent hepatocyte sensitization and possibly slower cell replication contribute toward the delayed or suppressed renewal of the liver parenchyma. Since liver regeneration is a highly organized and temporally regulated process, even slight deviations from the normal progression can substantially affect liver regeneration outcome[56]. In our hepatocyte-centric transcriptional study, these effects are reflected in changes in the proportion of control or ethanol LLM or PHx samples residing in different subpopulations. However, hepatic nonparenchymal cells, such as Kupffer cells and hepatic stellate cells, also play a significant role in the regulation of liver regeneration[57]. Sustained activation of nonparenchymal cells into pro- and antiregenerative phenotypes could determine the balance between normal and aberrant liver regeneration through microenvironmental changes and proportion shifts as seen in this study. An investigation involving identification of chronic ethanol-induced phenotype shifts in colocalized hepatocytes and nonparenchymal cells may shed light on the relative contributions of hepatocyte-intrinsic defects and external factors toward suppression of liver regeneration. As suggested in this study, hepatocyte transition propensities between the canonical molecular states in response to PHx could at least partly affect the liver regeneration outcome. Identifying marker genes that can predict adaptability of hepatocytes after chronic perturbations, although beyond the scope of this study, could likely prove to be an important first step toward resetting chronic perturbation-induced hepatocyte state transition propensities and point a way for improving surgical outcomes after liver resection.

ACKNOWLEDGMENTS: This work was financially supported by the National Institute of Biomedical Imaging and Bioengineering U01 EB023224, National Institute on Alcohol Abuse and Alcoholism R01 AA018873, and National Science Foundation EAGER 1747917. The funders had no role in the study design, data collection and analysis, decision to publish, or preparation of the manuscript. Author contributions: S.A., J.H., and R.V. conceived the study. S.A. and A.V. designed the experiments. S.A. performed the experiments. S.A. and A.V. analyzed the data and interpreted the results. A.S. and H.N. performed the immunofluorescence experiments and confocal imaging. A.S. performed tissue level protein measurements. S.A., A.V., J.H., and R.V. wrote the paper. All authors read and approved the final version of the manuscript. The authors declare no conflicts of interest.

REFERENCES

1. Tang F, Barbacioru C, Bao S, Lee C, Nordman E, Wang X, Lao K, Surani MA. Tracing the derivation of embryonic stem cells from the inner cell mass by single-cell RNA-seq analysis. Cell Stem Cell 2010;6(5):468–78.
2. Patel AP, Tirosh I, Trombetta JJ, Shalek AK, Gillespie SM, Wakimoto H, Cahill DP, Nahed BV, Curry WT, Martuza RL, et al. Single-cell RNA-seq highlights intratumoral heterogeneity in primary glioblastoma. Science 2014;344(6190):1396–401.
3. Amir ED, Davis KL, Tadmor MD, Simonds EF, Levine JH, Bendall SC, Shenfeld DK, Krishnaswamy S, Nolan GP, Pe'er D. viSNE enables visualization of high dimensional single-cell data and reveals phenotypic heterogeneity of leukemia. Nat Biotechnol. 2013;31(6):545.
4. Hough SR, Laslett AL, Grimmond SB, Kolle G, Pera MF. A continuum of cell states spans pluripotency and lineage commitment in human embryonic stem cells. PloS One 2009;4(11):e7708.
5. Park J, Brureau A, Kernan K, Starks A, Gulati S, Ogunnaike B, Schwaber J, Vadigepalli R. Inputs drive cell phenotype variability. Genome Res. 2014;24(6):930–41.
6. Guibentif C, Rönn RE, Böiers C, Lang S, Saxena S, Soneji S, Enver T, Karlsson G, Woods N. Single-cell analysis identifies distinct stages of human endothelial-to-hematopoietic transition. Cell Reports 2017;19(1):10–9.

7. Satija R, Farrell JA, Gennert D, Schier AF, Regev A. Spatial reconstruction of single-cell gene expression data. Nat Biotechnol. 2015;33(5):495.
8. Bendall SC, Davis KL, Amir ED, Tadmor MD, Simonds EF, Chen TJ, Shenfeld DK, Nolan GP, Pe'er D. Single-cell trajectory detection uncovers progression and regulatory coordination in human B cell development. Cell 2014; 157(3):714–25.
9. Llorens-Bobadilla E, Zhao S, Baser A, Saiz-Castro G, Zwadlo K, Martin-Villalba A. Single-cell transcriptomics reveals a population of dormant neural stem cells that become activated upon brain injury. Cell Stem Cell 2015; 17(3):329–40.
10. Halpern KB, Shenhav R, Matcovitch-Natan O, Tóth B, Lemze D, Golan M, Massasa EE, Baydatch S, Landen S, Moor AE. Single-cell spatial reconstruction reveals global division of labour in the mammalian liver. Nature 2017;542(7641):352.
11. Koteish A, Yang S, Lin H, Huang J, Diehl AM. Ethanol induces redox-sensitive cell-cycle inhibitors and inhibits liver regeneration after partial hepatectomy. Alcohol Clin Exp Res. 2002;26(11):1710–8.
12. Orrego H, Crossley IR, Saldivia V, Medline A, Varghese G, Israel Y. Long-term ethanol administration and short- and long-term liver regeneration after partial hepatectomy. J Lab Clin Med. 1981;97(2):221–30.
13. Kuttippurathu L, Juskeviciute E, Dippold RP, Hoek JB, Vadigepalli R. A novel comparative pattern analysis approach identifies chronic alcohol mediated dysregulation of transcriptomic dynamics during liver regeneration. BMC Genomics 2016;17(1):260.
14. Fausto N, Campbell JS, Riehle KJ. Liver regeneration. Hepatology 2006;43(S1):S45–53.
15. Michalopoulos GK. Liver regeneration. J Cell Physiol. 2007;213(2):286–300.
16. Michalopoulos GK. Liver regeneration after partial hepatectomy: Critical analysis of mechanistic dilemmas. Am J Pathol. 2010;176(1):2–13.
17. Taub R. Liver regeneration: From myth to mechanism. Nat Rev Mol Cell Biol. 2004;5(10):836.
18. Duguay L, Coutu D, Hetu C, Joly JG. Inhibition of liver regeneration by chronic alcohol administration. Gut 1982; 23(1):8–13.
19. Lieber CS, Decarli LM. Animal models of chronic ethanol toxicity. In: Packer L, editor. Methods in enzymology. Volume 233: Oxygen radicals in biological systems. San Diego (CA): Academic Press; 1994. p. 585–93.
20. Crumm S, Cofan M, Juskeviciute E, Hoek JB. Adenine nucleotide changes in the remnant liver: An early signal for regeneration after partial hepatectomy. Hepatology 2008; 48(3):898–908.
21. Untergasser A, Cutcutache I, Koressaar T, Ye J, Faircloth BC, Remm M, Rozen SG. Primer3—New capabilities and interfaces. Nucleic Acids Res. 2012;40(15):e115.
22. Koressaar T, Remm M. Enhancements and modifications of primer design program Primer3. Bioinformatics 2007;23(10):1289–91.
23. Ye J, Coulouris G, Zaretskaya I, Cutcutache I, Rozen S, Madden TL. Primer-BLAST: A tool to design target-specific primers for polymerase chain reaction. BMC Bioinformatics 2012;13(1):134.
24. Kamentsky L, Jones TR, Fraser A, Bray M, Logan DJ, Madden KL, Ljosa V, Rueden C, Eliceiri KW, Carpenter AE. Improved structure, function and compatibility for CellProfiler: Modular high-throughput image analysis software. Bioinformatics 2011;27(8):1179–80.
25. Andersen CL, Jensen JL, Orntoft TF. Normalization of real-time quantitative reverse transcription-PCR data: A model-based variance estimation approach to identify genes suited for normalization, applied to bladder and colon cancer data sets. Cancer Res. 2004;64(15):5245–50.
26. Vandesompele J, De Preter K, Pattyn F, Poppe B, Van Roy N, De Paepe A, Speleman F. Accurate normalization of real-time quantitative RT-PCR data by geometric averaging of multiple internal control genes. Genome Biol. 2002;3(7):research0034.
27. Troyanskaya O, Cantor M, Sherlock G, Brown P, Hastie T, Tibshirani R, Botstein D, Altman RB. Missing value estimation methods for DNA microarrays. Bioinformatics 2001;17(6):520–5.
28. Pavlidis P, Noble WS. Analysis of strain and regional variation in gene expression in mouse brain. Genome Biol. 2001;2(10):research0042.
29. Howe E, Holton K, Nair S, Schlauch D, Sinha R, Quackenbush J. MeV: Multiexperiment viewer. In: Ochs MF, Casagrande JT, Davuluri RV, editors. Biomedical informatics for cancer research. New York (NY): Springer; 2010. p. 267–78.
30. Maaten Lvd, Hinton G. Visualizing data using t-SNE. J Machine Learn Res. 2008;9:2579–605
31. Park J, Ogunnaike B, Schwaber J, Vadigepalli R. Identifying functional gene regulatory network phenotypes underlying single cell transcriptional variability. Prog Biophys Mol Biol. 2015;117(1):87–98.
32. Kraizer Y, Mawasi N, Seagal J, Paizi M, Assy N, Spira G. Vascular endothelial growth factor and angiopoietin in liver regeneration. Biochem Biophys Res Commun. 2001; 287(1):209–15.
33. Schwabe RF, Bradham CA, Uehara T, Hatano E, Bennett BL, Schoonhoven R, Brenner DA. c-Jun-N-terminal kinase drives cyclin D1 expression and proliferation during liver regeneration. Hepatology 2003;37(4):824–32.
34. Taniguchi E, Sakisaka S, Matsuo K, Tanikawa K, Sata M. Expression and role of vascular endothelial growth factor in liver regeneration after partial hepatectomy in rats. J Histochem Cytochem. 2001;49(1):121–9.
35. Koniaris LG, McKillop IH, Schwartz SI, Zimmers TA. Liver regeneration. J Am Coll Surg. 2003;197(4): 634–59.
36. Fausto N. Liver regeneration. J Hepatol. 2000;32:19–31.
37. Juskeviciute E, Dippold RP, Antony AN, Swarup A, Vadigepalli R, Hoek JB. Inhibition of miR-21 rescues liver regeneration after partial hepatectomy in ethanol-fed rats. Am J Physiol Gastrointest Liver Physiol. 2016;311(5): G794–806.
38. Rosa JL, Bartrons R, Tauler A. Gene expression of regulatory enzymes of glycolysis/gluconeogenesis in regenerating rat liver. Biochem J. 1992;287(Pt 1):113–6.
39. Wang G, Chen QM, Minuk GY, Gong Y, Burczynski FJ. Enhanced expression of cytosolic fatty acid binding protein and fatty acid uptake during liver regeneration in rats. Mol Cell Biochem. 2004;262(1–2):41–9.
40. Cederbaum AI. Alcohol metabolism. Clin Liver Dis. 2012; 16(4):667–85.
41. Roberts BJ, Song BJ, Soh Y, Park SS, Shoaf SE. Ethanol induces CYP2E1 by protein stabilization. Role of ubiquitin conjugation in the rapid degradation of CYP2E1. J Biol Chem. 1995;270(50):29632–5.

42. Charlton M, Viker K, Krishnan A, Sanderson S, Veldt B, Kaalsbeek A, Kendrick M, Thompson G, Que F, Swain J. Differential expression of lumican and fatty acid binding protein-1: New insights into the histologic spectrum of nonalcoholic fatty liver disease. Hepatology 2009;49(4): 1375–84.
43. Colell A, García-Ruiz C, Miranda M, Ardite E, Marí M, Morales A, Corrales F, Kaplowitz N, Fernández-Checa JC. Selective glutathione depletion of mitochondria by ethanol sensitizes hepatocytes to tumor necrosis factor. Gastroenterology 1998;115(6):1541–51.
44. Riehle KJ, Campbell JS, McMahan RS, Johnson MM, Beyer RP, Bammler TK, Fausto N. Regulation of liver regeneration and hepatocarcinogenesis by suppressor of cytokine signaling 3. J Exp Med. 2008;205(1):91–103.
45. Hoek JB, Pastorino JG. Ethanol, oxidative stress, and cytokine-induced liver cell injury. Alcohol 2002;27(1): 63–8.
46. Kuttippurathu L, Patra B, Hoek JB, Vadigepalli R. A novel comparative pattern count analysis reveals a chronic ethanol-induced dynamic shift in immediate early NF- B genome-wide promoter binding during liver regeneration. Molecular BioSystems 2016;12(3):1037–56.
47. Verma A, Makadia H, Hoek JB, Ogunnaike BA, Vadigepalli R. Computational modeling of spatiotemporal Ca(2+) signal propagation along hepatocyte cords. IEEE Trans Biomed Eng. 2016;63(10):2047–55.
48. Huang S, Eichler G, Bar-Yam Y, Ingber DE. Cell fates as high-dimensional attractor states of a complex gene regulatory network. Phys Rev Lett. 2005;94(12):128701.
49. Marco E, Karp RL, Guo G, Robson P, Hart AH, Trippa L, Yuan GC. Bifurcation analysis of single-cell gene expression data reveals epigenetic landscape. Proc Natl Acad Sci USA 2014;111(52):E5643–50.
50. Guo G, Huss M, Tong GQ, Wang C, Sun LL, Clarke ND, Robson P. Resolution of cell fate decisions revealed by single-cell gene expression analysis from zygote to blastocyst. Dev Cell 2010;18(4):675–85.
51. Park J, Zhu H, O'Sullivan S, Ogunnaike BA, Weaver DR, Schwaber JS, Vadigepalli R. Single-cell transcriptional analysis reveals novel neuronal phenotypes and interaction networks involved in the central circadian clock. Front Neurosci. 2016;10:481.
52. Rothenberg ME, Kalisky T, Dalerba PD, Nusse Y, Quake S, Clarke MF. Single cell gene expression profiling of adult murine colon provides novel insight into both the origin of stem cells and their supportive cell type. Gastroenterology 2011;140(5):S13–4.
53. Reif R, Ghallab A, Beattie L, Günther G, Kuepfer L, Kaye PM, Hengstler JG. In vivo imaging of systemic transport and elimination of xenobiotics and endogenous molecules in mice. Arch Toxicol. 2017;91(3):1335–52.
54. Zimmerman BT, Crawford GD, Dahl R, Simon FR, Mapoles JE. Mechanisms of acetaldehyde-mediated growth inhibition: Delayed cell cycle progression and induction of apoptosis. Alcohol Clin Exp Res. 1995;19(2):434–40.
55. Holownia A, Ledig M, Mapoles J, Ménez J. Acetaldehyde-induced growth inhibition in cultured rat astroglial cells. Alcohol 1996;13(1):93–8.
56. Kuttippurathu L, Parrish A, Vadigepalli R. Integrated computational model of intracellular signaling and microRNA regulation predicts the network balances and timing constraints critical to the hepatic stellate cell activation process. Processes 2014;2(4):773–94.
57. Cook D, Ogunnaike BA, Vadigepalli R. Systems analysis of non-parenchymal cell modulation of liver repair across multiple regeneration modes. BMC Systems Biol. 2015;9(1):71.